

## Two-dimensional Hubbard-Holstein model

E. Berger, P. Valášek, and W. von der Linden

*Max-Planck-Institut für Plasmaphysik, EURATOM Association, D-85740 Garching bei München, Germany*

(Received 13 March 1995)

The interplay of electron-phonon coupling and strong electronic correlations is studied in the frame of the two-dimensional Hubbard-Holstein model. Static and dynamic properties are determined by quantum Monte Carlo simulations and by Migdal-Eliashberg theory. The comparison allows us to assess the diagrammatic approach. The competition between the phonon-mediated electron-electron attraction and the local Coulomb repulsion leads to a rich phase diagram, which we study in detail for a wide range of parameters. We address the question, to which extent the systems can be described by an effective negative- $U$  Hubbard model.

### I. INTRODUCTION

The two-dimensional Holstein model<sup>1</sup> has been the subject of intense numerical and analytic studies. It is particularly appealing, as, on the one hand, its physical properties can be determined for a wide range of parameters by approximation-free quantum-Monte-Carlo (QMC) simulations, which allow us to study both the physics of the model and the reliability of standard diagrammatic techniques; on the other hand, the Holstein model possesses a rich and interesting phase diagram covering, e.g., charge-density wave (CDW) and superconductivity (SC) as observed, e.g., in  $\text{Ba}_{1-x}\text{K}_x\text{BiO}_3$ , which exhibits a CDW-driven metal-insulator transition and which, upon doping with Pb or K, becomes superconducting. The Holstein model is also particularly interesting as it represents one of the rare models in which a departure from Fermi-liquid behavior occurs. Here the electronic spectral density loses the quasiparticle peak and is swamped by an incoherent background with increasing electron-phonon coupling.<sup>2,3</sup> The significance of the Holstein model is strongly increased by the fact that the one-dimensional model with linear electronic dispersion is one of the very few many-body models which has been solved exactly.<sup>4</sup> Much of the physics of the bare Holstein model in two dimensions has been elaborated by QMC simulations and diagrammatic studies, based on Migdal-Eliashberg theory.<sup>3,5-12</sup> For half filling and strong electron-phonon coupling the Holstein model maps onto an effective-attractive Hubbard model. Consequently, CDW and on-site  $s$ -wave superconductivity coexist. Away from half filling, the superconducting phase dominates. Likewise, with decreasing electron-phonon coupling or increasing phonon frequency, superconductivity is favored. Recent progress in the field of QMC simulations has made it possible to determine dynamic properties. Those computations established a gap in the electronic spectrum at the Fermi surface.<sup>5,9,11</sup> As far as Migdal-Eliashberg (ME) theory<sup>13</sup> is concerned, Marsiglio<sup>3,7</sup> found a strikingly good agreement with QMC data, if only the ME equations are solved without further approximations. Even the departure from Fermi-liquid behavior can be reproduced. The CDW gap, however,

cannot be described by ME as long as translational invariance is retained.

Here we supplement the discussion of the physical properties of the Holstein model. A feature missing in the Holstein model is the Coulomb repulsion of electrons. Particularly in view of the high-temperature superconductors, the question arises, to which extent strong electronic correlations influence electron-phonon mediated superconductivity. Put differently, how does the electron-phonon coupling act in a system which departs from a Fermi liquid? To study these questions, we add a repulsive Hubbard term to the Holstein model. Exact results for the combined Hubbard-Holstein model are only available for two sites, which are studied in great detail by Ranninger and co-workers<sup>14,15</sup> and for the dilute limit of 1 and 2 electrons in a one-dimensional (1D) chain by exact diagonalization.<sup>16</sup> Here we will extend these studies to 2D systems and explore the vicinity of half filling.

### II. MODEL

The Hubbard-Holstein model is described by the Hamiltonian

$$H = \underbrace{-t \sum_{\langle i,j \rangle, \sigma} c_{i,\sigma}^\dagger c_{j,\sigma}}_{H_{\text{kin}}} + \underbrace{U \sum_i n_{i,\uparrow} n_{i,\downarrow}}_{H_{\text{Hub}}} + \underbrace{\omega_0 \sum_i a_i^\dagger a_i + g \sum_i n_i (a_i^\dagger + a_i)}_{H_{e\text{-ph}}}. \quad (1)$$

The various parts are as follows: nearest-neighbor hopping of electrons  $H_{\text{kin}}$ ; Hubbard interaction  $H_{\text{Hub}}$  with on-site Coulomb repulsion  $U$ ; kinetic energy of Einstein phonons of frequency  $\omega_0$ , and electron-phonon interaction of strength  $g$  summarized in  $H_{e\text{-ph}}$ .  $c_{i,\sigma}^\dagger$  ( $c_{i,\sigma}$ ) are the ubiquitous creation (annihilation) operators for electrons of spin  $\sigma$  at site  $i$ , and  $a_i^\dagger$  ( $a_i$ ) are the analogous operators for phonons. In the model under consideration, the electrons couple through the density  $n_{i,\sigma} = c_{i,\sigma}^\dagger c_{i,\sigma}$  to the local phonon displacement  $(a_i^\dagger + a_i)$ . The Holstein model  $H_{\text{kin}} + H_{e\text{-ph}}$  and the Hubbard model  $H_{\text{kin}} + H_{\text{Hub}}$  are lim-

iting cases for  $g=0$  and  $U=0$ , respectively. In the following, all energies are expressed in units of  $t$ . The model shows a rich variety of different phases. Charge- and spin-density waves,<sup>5</sup> as well as a metal-insulator transition<sup>11</sup> and SC, are found in numerical and analytical treatments. Upon integrating out the phonon degrees of freedom, an effective electron-electron interaction is obtained that contains the Hubbard and a phonon-mediated part. It is determined in second-order perturbation theory by

$$V_{e-e}^{\text{eff}}(\omega) = U - \frac{2g^2\omega_0}{\omega_0^2 - \omega^2}.$$

In the adiabatic limit  $\omega_0 \rightarrow \infty$  the retarded interaction maps onto an instantaneous Hubbard interaction with

$$V_{e-e}^{\text{eff}} = U - 2g^2/\omega_0.$$

Hence there is a competition between the Coulomb repulsion  $U$  and the electron-phonon interaction, but, due to the retardation of the phonon-mediated part, the physics of the Hubbard-Holstein model is expected to deviate in general from that of an effective Hubbard model.

### III. FORMALISM AND MEASURED QUANTITIES

#### A. Migdal-Eliashberg theory

In ME theory, electron and phonon Green's functions are determined for imaginary frequencies by

$$G_{\sigma}(k, i\omega_n) = \frac{1}{i\omega_n - \epsilon_k + \mu - \Sigma_{\sigma}(k, i\omega_n)}, \quad (2)$$

$$D(q, i\nu_n) = \frac{2\omega_0}{(i\nu_n)^2 - \omega_0^2 - 2\omega_0\Pi(q, i\nu_n)}, \quad (3)$$

with Matsubara frequencies  $\omega_n = (2n+1)\pi/\beta$  for fermions and  $\nu_n = 2n\pi/\beta$  for bosons. We use renormalized Migdal-Eliashberg theory for computing the self-energies. The diagrams of the renormalized ME equations for the bare Holstein model are shown in Fig. 1. In this approximation vertex corrections are neglected. Routinely, unrenormalized phonons are used (UME), which amounts to ignoring the phonon self-energy. In the usual approach phonon renormalization is accounted for—in an uncontrolled way though—by using experimental phonon dispersions. Likewise, vertex corrections

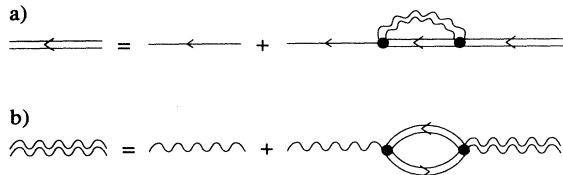


FIG. 1. The Migdal-Eliashberg equations in diagrammatic form for electrons (a) and phonons (b). The single (double) solid line represents the noninteracting (interacting) electron Green's function, the single (double) wavy line the noninteracting (interacting) phonon Green's function. The vertex point represents the emission and absorption of a phonon.

are partly included through an effective electron-phonon coupling  $g^{\text{eff}}$ . The self-energies for electrons and phonons in ME, entering Eqs. (2) and (3), are

$$\Sigma_{\sigma}(k, i\omega_n) = -\frac{g^2}{\beta N} \sum_{k', n'} D(k-k', i\omega_n - i\omega_{n'}) G_{\sigma}(k', i\omega_{n'}), \quad (4)$$

$$\Pi(q, i\nu_n) = \frac{g^2}{\beta N} \sum_{k', n', \sigma'} G_{\sigma'}(k'+q, i\omega_{n'} + i\nu_n) G_{\sigma'}(k', i\omega_{n'}). \quad (5)$$

We treat electron correlations on the same footing by neglecting vertex corrections and by including only density fluctuation (RPA) diagrams.<sup>17-19</sup> Figure 2 shows the diagrammatic form of the Migdal-Eliashberg equations for the Hubbard-Holstein model. In addition to the diagrams for the bare Holstein model, we take into account the screening of the electron-electron and the electron-phonon interaction. Summation of all combinatorially possible diagrams to infinite order yields<sup>20</sup>

$$\Sigma_{\sigma}(k, i\omega_n) = -\frac{1}{\beta N} \sum_{k', n'} G_{\sigma}(k-k', i\omega_n - i\nu_{n'}) \times \left[ \frac{g^2 D(k', i\nu_{n'})}{[1 - U\chi(k', i\nu_{n'})]^2} + \frac{U^2 \chi(k', i\nu_{n'})}{1 - [U\chi(k', i\nu_{n'})]^2} \right], \quad (6)$$

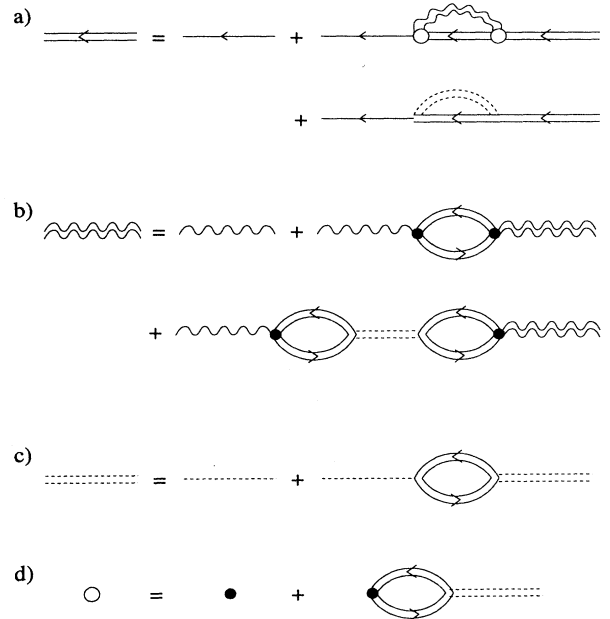


FIG. 2. The ME equations for the Hubbard-Holstein model for electrons (a) and phonons (b). The single (double) solid line represents the noninteracting (interacting) electron Green's function, the single (double) wavy line the noninteracting (interacting) phonon Green's function. The vertex point represents the emission and absorption of a phonon. Also depicted is the screened electron-electron interaction (c) and the effective electron-phonon interaction (d).

$$\Pi(q, i\nu_n) = \frac{2g^2 \chi(q, i\nu_n)}{1 - U\chi(q, i\nu_n)}, \quad (7)$$

with

$$\chi(q, i\nu_n) = \frac{1}{\beta N} \sum_{k', n'} G(k' + q, i\omega_{n'} + i\nu_n) G(k', i\omega_{n'}). \quad (8)$$

The regular Migdal-Eliashberg theory is recovered for  $U=0$ . The chemical potential  $\mu$  is fixed by the filling

$$\langle n \rangle = 1 + \frac{1}{\beta N} \sum_{k', n', \sigma'} G_{\sigma'}(k', i\omega_{n'}).$$

One-particle excitations are described by the spectral functions

$$A_{\sigma}(k, \omega) = -\frac{1}{\pi} \text{Im} G_{\sigma}(k, \omega + \mu) \text{sgn}(\omega)$$

and

$$B(q, \nu) = -\frac{1}{\pi} \text{Im} D(q, \nu) \text{sgn}(\nu),$$

respectively.  $G_{\sigma}(k, \omega + \mu)$  and  $D(q, \nu)$  are the analytic continuations of the Matsubara functions to the real-frequency axis. They are routinely performed in this context by the Padé approximation.<sup>21</sup> It should be noted that the analytic continuation does not have a unique solution, since data are only available for a limited number of imaginary frequencies. If applied carefully, i.e., using enough Matsubara frequencies and performing a thorough study of the  $\beta$  dependence, the Padé approximation works, however, extremely well.<sup>20</sup> The poles of Eq. (3) define the renormalized phonon frequency

$$\Omega(q, i\nu_n) = \sqrt{\omega_0^2 + 2\omega_0 \Pi(q, i\nu_n)}.$$

The static electronic density-density susceptibility shows that the Holstein model has a tendency towards a CDW phase. Within ME theory, the CDW susceptibility is found by summing all bubble diagrams, as indicated in Fig. 3. This yields

$$\chi^{\text{CDW}}(q) = \frac{\chi_0^{\text{CDW}}(q)}{1 - \frac{2g^2}{\omega_0} \chi_0^{\text{CDW}}(q)}, \quad (9)$$

with

$$\chi_0^{\text{CDW}}(q) = -\frac{\Pi(q, 0)}{g^2}. \quad (10)$$

It has been pointed out by Marsiglio<sup>3,6</sup> that, based on CDW susceptibilities, the self-consistent phonon renormalization plays a crucial role in accounting for a proper phase transition. The agreement between QMC and ME



FIG. 3. Bubble diagrams representing the CDW susceptibility.

susceptibilities is remarkably close if phonons are renormalized and Green's functions are evaluated self-consistently.

### B. Projector quantum Monte Carlo

Beside the diagrammatic technique, we employ the projector quantum-Monte-Carlo (PQMC) method<sup>22-24</sup> to compute ground-state properties. It is an approximation-free numerical method which gives exact results up to a statistical error, which can be reduced by increasing the sample size. The basic idea of PQMC is to project the exact many-body ground state  $|0\rangle = \lim_{\theta \rightarrow \infty} e^{-\theta H} |\Psi_T\rangle$  out of a suitable trial function  $|\Psi_T\rangle$ . For a numerical treatment one chooses a large but finite  $\theta$ . The result will be a mixture of low-lying excited states within an energy window of width  $\sim 1/\theta$ .  $\theta$  is chosen such that the ground-state plateau is reached. The electronic part of the PQMC scheme has already been discussed in great detail by Sorella *et al.*<sup>22</sup> The phononic degrees of freedom are treated in the same way as proposed by Hirsch.<sup>25</sup> In first quantization we integrate out the phonon momenta. This procedure leads to an effective local potential for the electrons depending on the phonon displacements.<sup>25</sup> Hence, expectation values

$$\langle \mathbf{A} \rangle = \frac{\langle \Psi_T | e^{-\beta H} \mathbf{A} e^{-\beta H} | \Psi_T \rangle}{\langle \Psi_T | e^{-2\beta H} | \Psi_T \rangle} \quad (11)$$

are mapped onto megadimensional sums over Ising variables from the Hubbard-Stratonovich transformation and over continuous phonon displacements. Each of these quantities is defined on a  $(2+1)$ -dimensional space-time lattice. The sums are determined by importance sampling Monte Carlo.<sup>23</sup> The phonon Green's functions in real space with  $\mathbf{T}$  as time-ordering operator read

$$D(i, j, \tau) = -\mathbf{T} \langle x_i(\tau) x_j(0) \rangle, \quad (12)$$

$$D(q, \tau) = -\mathbf{T} \langle A(q, \tau) A(-q, 0) \rangle, \quad (13)$$

with

$$A(q, \tau) = e^{\tau H} (a_q + a_{-q}^\dagger) e^{-\tau H}. \quad (14)$$

In order to measure time-dependent quantities—which is amenable in this scheme only for imaginary times—we discretize the time-evolution operator  $\exp(-\tau H)$  into small time slices. The phonon Green's function for imaginary times  $\tau_n = n\Delta\tau$ , on the time grid provided by the Trotter-Suzuki decomposition, reads

$$D(q, \tau_n) = -\langle \Psi_T | e^{-m\Delta\tau H} e^{n\Delta\tau H} A(q, 0) e^{-n\Delta\tau H} \times A(-q, 0) e^{-m\Delta\tau H} | \Psi_T \rangle. \quad (15)$$

This means we have  $m$  Trotter times to project out the ground-state function and a time window of  $n$  time slices to measure the dynamics of the system. Details are given in Ref. 26. For  $T=0$  the phonon Green's function is related to the spectral weight  $B(q, \nu)$  and the density of states  $F(\nu)$  via

$$D(q, \tau) = - \int_0^\infty d\nu e^{-\tau\nu} B(q, \nu), \quad (16)$$

$$D(i, i; \tau) = - \int_0^\infty d\nu e^{-\tau\nu} F(\nu),$$

respectively. The inversion is utterly ill posed due to incomplete and noisy data, which hampered the determination of dynamic properties from QMC simulations for many years. Recently, Silver and co-workers<sup>27</sup> suggested the maximum entropy method (MaxEnt), which had proven successful in a wide range of data-analysis problems<sup>28</sup> before. It is based on Bayesian probability theory<sup>29</sup> and provides a consistent theoretical frame for using probability theory as logic. The static Green's function is obtained from the imaginary time data by

$$D(q, i\nu_n = 0) = \int_0^\beta D(q, \tau) d\tau.$$

In PQMC simulations equal-time correlation functions are most easily accessible:

$$C = \langle OO^\dagger \rangle.$$

For the charge- and spin-density waves the operator  $O$  reads

$$O_{\text{CDW}} = \rho_q = \frac{1}{\sqrt{N}} \sum_{l, \sigma} e^{iq_l} n_{l\sigma},$$

$$O_{\text{SDW}} = S_q^z = \frac{1}{\sqrt{N}} \sum_l e^{iq_l} \frac{1}{2} (n_{l, \uparrow} - n_{l, \downarrow}).$$

Off-diagonal long-range order (ODLRO) is detected by the zero-momentum pair-field operator

$$O = \Delta_\alpha = \frac{1}{\sqrt{N}} \sum_i \Delta_\alpha(i). \quad (17)$$

The latter is used to measure spatial coherence between pair-field creation and annihilation for three different symmetries  $\alpha$ : (a) on-site  $s$  wave,

$$\Delta_s(i) = c_{i, \uparrow} c_{i, \downarrow},$$

(b) extended  $s$  wave,

$$\Delta_{s^*}(i) = \sum_\delta (c_{i+\delta, \uparrow} c_{i, \downarrow} - c_{i+\delta, \downarrow} c_{i, \uparrow}) / \sqrt{8},$$

and (c)  $d_{x^2-y^2}$  wave,

$$\Delta_d(i) = \sum_\delta \cos(\pi\delta_x) (c_{i+\delta, \uparrow} c_{i, \downarrow} - c_{i+\delta, \downarrow} c_{i, \uparrow}) / \sqrt{8}.$$

The sums are restricted to nearest-neighbor vectors  $\delta$ . Results will be depicted for the vertex correlation functions, in which single-particle renormalization effects are removed by subtracting the zero-order bubble.<sup>30</sup> A positive (negative) pair-field vertex indicates an effective attractive (repulsive) interaction. We are particularly interested in the distance dependence of the pair-field correlation function

$$\chi(x_l) = \frac{1}{N} \sum_i \langle \Delta_\alpha(i+l) \Delta_\alpha(i) \rangle,$$

to study whether the system has ODLRO, i.e.,

$$\chi(x_l) \xrightarrow{|x_l| \rightarrow \infty} C > 0,$$

and therefore tends to a SC phase in the thermodynamic limit.

## IV. RESULTS

### A. Charge- and spin-density waves

We start out with the analysis of charge-density waves. To allow for a comparison of QMC and ME data, results are given for  $4 \times 4$  lattices with periodic boundary conditions. QMC and ME predict unanimously a CDW phase at half filling with a pronounced peak in the CDW structure factor at  $q_0 = (\pi, \pi)$ . The peak height increases with increasing electron-phonon coupling  $g$ . This behavior is depicted in Fig. 4, where we plot the dependence of  $\chi^{\text{CDW}}$  versus  $g$ . There we also show the filling dependence.  $\chi_{q_0}^{\text{CDW}}$  decreases rapidly with hole doping and is negligibly small for  $\langle n \rangle = 0.5$ , due to a general decrease of the susceptibility and a shift of the peak away from  $q_0$ . This tendency is observed in the CDW correlation function as well. For fixed  $g^2/\omega_0$  the CDW susceptibility increases with decreasing  $\omega_0$  as the effective electron-electron interaction becomes more and more retarded.<sup>20</sup> The Hubbard interaction, which reduces charge fluctuations, counteracts the formation of charge-density waves. This behavior is predicted by QMC and ME. Figure 5 shows the result obtained by ME. The  $U$  dependence of the static susceptibility can be described accurately by an exponential dependence  $\chi_{q_0}^{\text{CDW}}(U) \approx \chi_{q_0}^{\text{CDW}}(U=0) e^{-U/U_0}$ . For  $g = \omega_0 = 0.5$ , ME yields  $U_0 = 0.75$ . The situation is, however, different away from half filling. For  $n = 0.875$  and  $U = 0$ , QMC data<sup>10</sup> reveal that the peak in the CDW structure is shifted away from the nesting-vector  $q_0$  towards  $q = (\pi/2, \pi/2)$ . In this instance, the influence of the local Coulomb repulsion is opposite: it shifts the

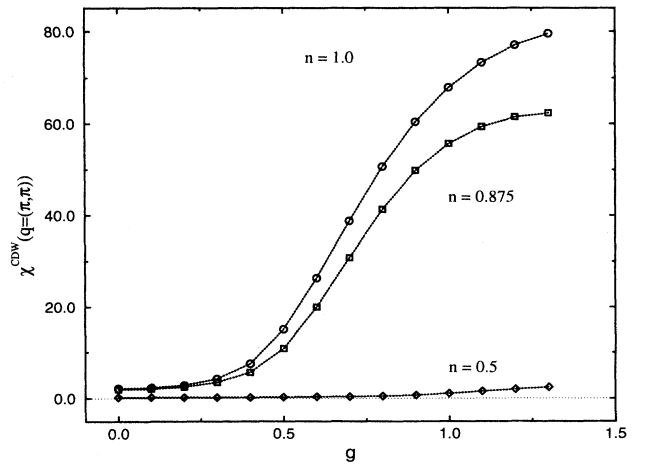


FIG. 4. The  $g$  dependence of the CDW susceptibility for the fillings  $\langle n \rangle = 1, 0.875$ , and  $0.5$ , for parameters  $q = q_0$ ,  $\omega_0 = 0.5$ , and  $\beta = 10$  on a  $4 \times 4$  lattice.

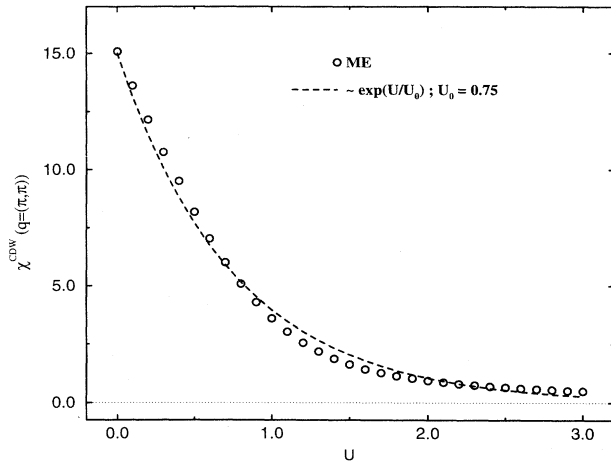


FIG. 5. The dependence of the CDW susceptibility upon  $U$  for the parameters  $q=q_0$ ,  $g=0.5$ ,  $\omega_0=0.5$ , and  $\beta=10$  on a  $4 \times 4$  lattice.

CDW peak back to  $q_0$ , leading to an increasing  $\chi_{q_0}^{\text{CDW}}$ . Within ME we determined the CDW transition temperature from the  $T$  dependence of  $1/\chi_{q=(\pi,\pi)}^{\text{CDW}}$  for a  $4 \times 4$  lattice and parameters  $\omega_0=1$ ,  $g^2/\omega_0=1$ , and  $U=0$ . QMC simulations<sup>7</sup> for an  $8 \times 8$  system yield  $kT_C \approx 0.1$ , which is greatly overestimated ( $kT_C=0.7$ ) by RPA or UME. A significant improvement ( $kT_C=0.2$ ) is achieved by an exact treatment of ME theory. Nonetheless, the result is still a factor 2 off, which has to be attributed mainly to vertex corrections.

The spin-density wave shows the expected behavior for large Hubbard interaction.<sup>5</sup> In the half-filled case the antiferromagnetic structure factor increases with increasing Hubbard  $U$  and it vanishes with doping or increasing  $g^2/\omega_0$ .

### B. Renormalized phonon frequency

Due to the pronounced susceptibility of the system towards a staggered density fluctuation, the frequency of the  $q_0$  phonon is weakened and approaches zero at the CDW phase boundary. We have calculated the effective phonon frequency

$$\Omega(q, i\nu_n=0) = \sqrt{\omega_0^2 + 2\omega_0\Pi(q, i\nu_n=0)} \quad (18)$$

with QMC, ME, and RPA for two different wave vectors  $q$ :  $q=q_0$  and  $q=(\pi, \pi/2)$ . In Figs. 6 and 7 the results are depicted for half filling. ME and QMC yield that for  $q=q_0$  the frequency approaches zero very rapidly, whereas for  $q=(\pi, \pi/2)$  it remains at finite value. It appears that the effective phonon frequency in the Holstein model is fairly well described by renormalized ME theory, while the RPA results start to deviate as soon as the system approaches the CDW phase. The  $U$  dependence of the phonon frequency is depicted in Fig. 8 for half filling and  $q_0$ . The Hubbard repulsion increases the phonon frequency, since  $U$  counteracts the effect of the electron-phonon interaction. With doping, the CDW

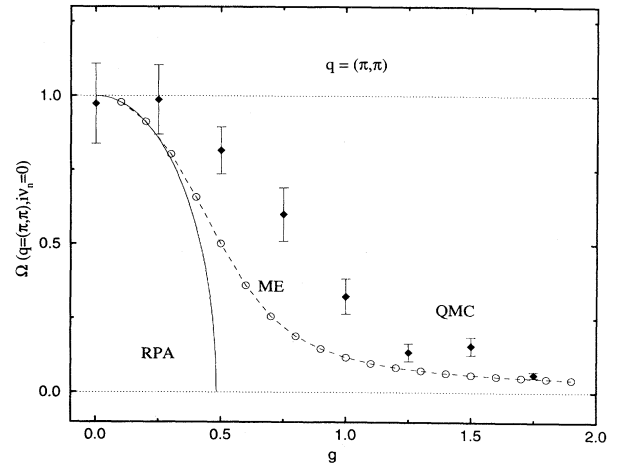


FIG. 6. The effective phonon frequency  $\Omega$  as a function of  $g$  for parameters  $\omega_0=1$ ,  $\beta=10$ ,  $q=q_0$ , and  $\langle n \rangle=1$ . The straight line shows the RPA result, the circles are obtained with ME, and the squares are QMC data.

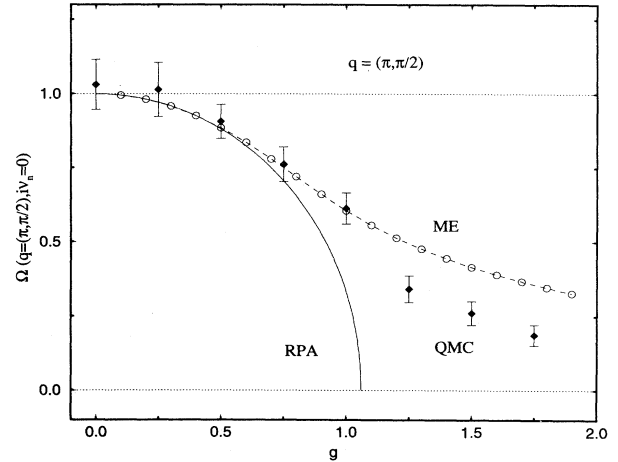


FIG. 7. The effective phonon frequency  $\Omega$  as a function of  $g$  for parameters  $\omega_0=1$ ,  $\beta=10$ ,  $q=(\pi, \pi/2)$ , and  $\langle n \rangle=1$ .

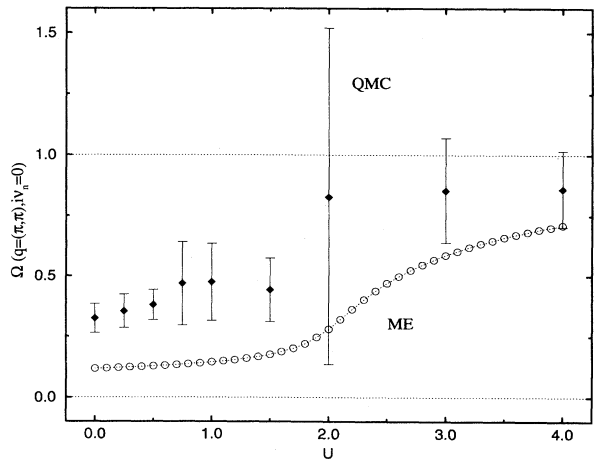


FIG. 8. The  $U$  dependence of the renormalized phonon frequency for  $q=(\pi, \pi)$  and  $q=(\pi, \pi/2)$ .  $\omega_0=4$ ,  $g=1$ ,  $\beta=10$ , and  $\langle n \rangle=1$ .

peak is shifted away from  $q_0$ , which brings back the frequency of the  $q_0$  phonon towards  $\omega_0$ . In this case the Coulomb repulsion leads to a significant softening of the phonon mode.

### C. Phonon spectral function

Also, the behavior of the phonon spectral density  $B(q, \nu)$  [Eq. (16)], as obtained by QMC and ME theory, depends strongly on the wave vector  $q$ . Figure 9 shows the  $g$  dependence of  $B(q=q_0, \nu)$  for  $U=0$  and half filling. For  $g=0$ , the spectral density is peaked at the bare phonon frequency  $\omega_0$ . The finite width is due to the Padé approximation. Turning on  $g$  leads to a broadening and a slight shift to a lower frequency. Simultaneously, a second peak develops at  $\omega \approx 0$  which dominates the spectral density for  $g \gtrsim \omega_0$ . This scenario can be explained in a single-mode approximation.<sup>17</sup> Turning on  $U$  (Fig. 10) causes a reversed behavior: The peak at  $\omega \approx 0$  disappears, while the peak at  $\omega \lesssim \omega_0$  shifts back to higher frequencies and becomes sharper. For  $q$  vectors away from  $q_0$ ,  $B(q, \nu)$  retains a pronounced single pole structure, which is merely shifted to lower frequencies with increasing  $g$ . With increasing  $U$  the peak in the spectral density is shifted back towards  $\omega_0$ . Away from half filling the behavior is different. In Fig. 11 we show the phonon spectral density for  $\langle n \rangle = 0.875$  and  $q_0$ . Increasing  $U$  leads in this case to a softening of the phonon peak, contrary to our finding for half filling. The behavior is due to the shift of the peak in the CDW structure factor as depicted in Fig. 12.

### D. Electron spectral function

Next, we consider the effect of the electron-phonon coupling and the electron-electron interaction on electronic properties. It has been shown<sup>9</sup> by QMC studies for

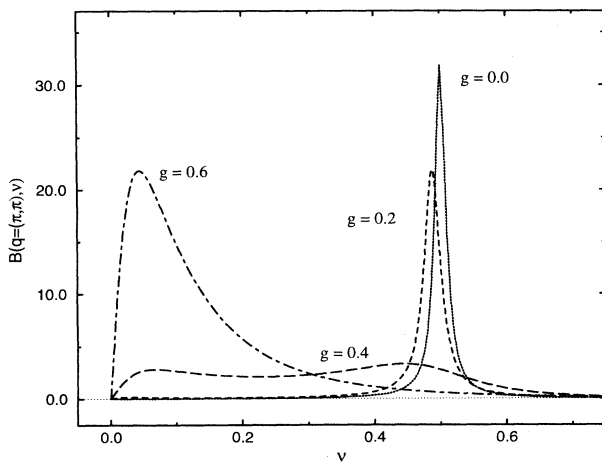


FIG. 9. The spectral density of the phonons as found by ME for different values of the electron-phonon coupling  $g$  for  $\omega_0=0.5$ ,  $\beta=10$ ,  $\langle n \rangle=1$ , and  $q=(\pi, \pi)$ . The dotted line corresponds to  $g=0$ , the dashed line to  $g=0.2$ , the long dashed line to  $g=0.4$ , and the dot-dashed line to  $g=0.6$ .

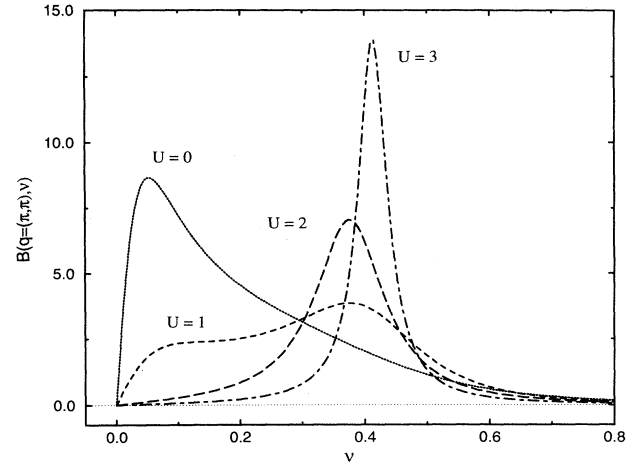


FIG. 10. The spectral density of the phonons as found by ME for different values of the Hubbard interaction  $U$  for  $\omega_0=0.5$ ,  $g=0.5$ ,  $\beta=10$ ,  $\langle n \rangle=1$ , and  $q=(\pi, \pi)$ . The dotted line corresponds to  $U=0$ , the dashed line to  $U=1$ , the long dashed line to  $U=2$ , and the dot-dashed line to  $U=3$ .

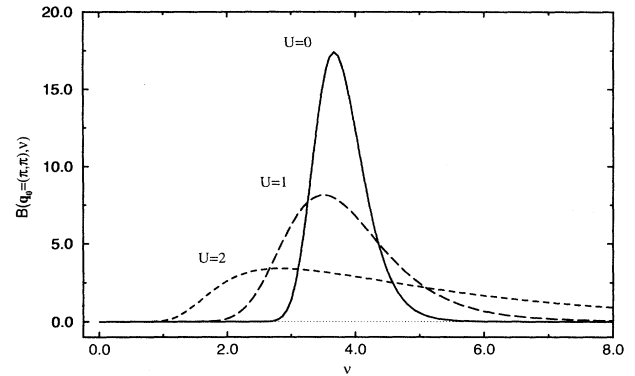


FIG. 11. The phonon spectral weight function  $B(q, \nu)$  as obtained by QMC for  $\langle n \rangle = 0.875$  with  $g=1$ ,  $\omega_0=4$  on a  $4 \times 4$  lattice. The momentum is  $q=q_0=(\pi, \pi)$ . The lines show the behavior of the phonon renormalization with increasing local repulsion  $U$ .

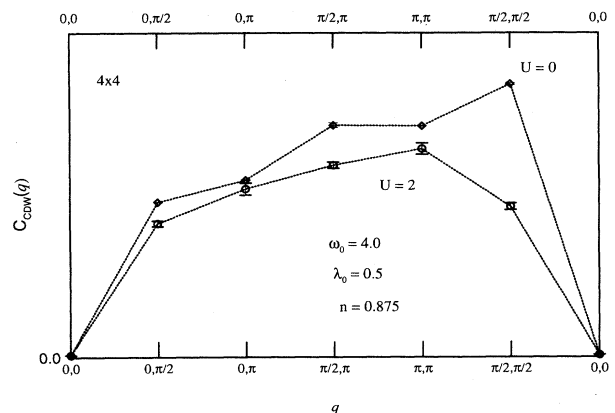


FIG. 12. The CDW structure factor for  $\langle n \rangle = 0.875$ ,  $g=1$ ,  $\lambda_0=2g^2/\omega_0$ ,  $\omega_0=4$  on a  $4 \times 4$  lattice and  $U=0$  with its incommensurate peaks obtained by QMC. An increasing repulsion shifts the electron density structure back to  $q_0=(\pi, \pi)$ .

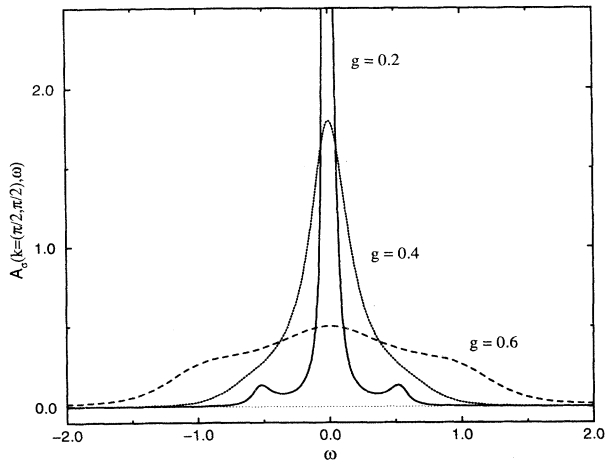


FIG. 13. The ME electronic spectral density for different values of  $g$  for parameters  $\omega_0=0.5$ ,  $\beta=10$ ,  $\langle n \rangle=1$ , and  $k=(\pi/2, \pi/2)$ . The straight line gives the result for  $g=0.2$ , the dotted line for  $g=0.4$ , and the dashed line for  $g=0.6$ .

$U=0$  that the electronic self-energy behaves differently depending on the  $k$  vectors. For  $k$ 's on the Fermi surface the self-energy diverges upon approaching  $\omega=0$  along the imaginary axis, which indicates the existence of a CDW gap. For wave vectors away from the Fermi surface the gap vanishes. The ME results yield the same behavior of the self-energy. It should be mentioned that in a finite  $4 \times 4$  system there cannot be a real divergence in the self-energy. We observed, however, that with increasing  $g$  it tends more and more towards a divergence. The temperature and  $g$  dependence of the gap have been studied directly in terms of the spectral density for real frequencies upon combining QMC and MaxEnt.<sup>11</sup> The electronic spectral density obtained by ME theory for  $U=0$  and a wave vector on the Fermi surface is shown in

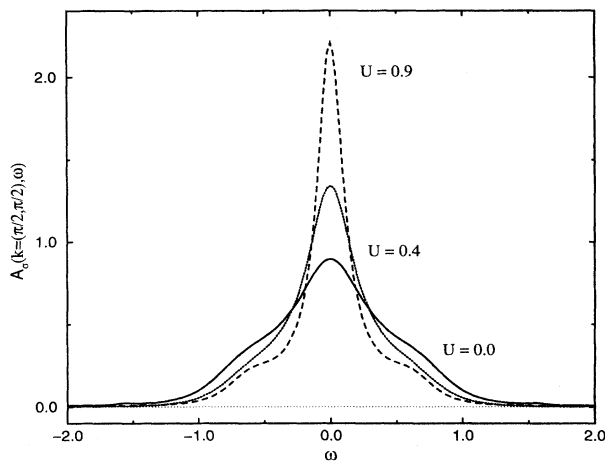


FIG. 14. The  $U$  dependence of the electronic spectral density for parameters  $\omega_0=0.5$ ,  $g=0.5$ ,  $\beta=10$ ,  $\langle n \rangle=1$ , and  $k=(\pi/2, \pi/2)$  as obtained by ME for a  $4 \times 4$  lattice. The straight line gives the result for  $U=0$ , the dotted line for  $U=0.4$ , and the dashed line for  $U=0.9$ .

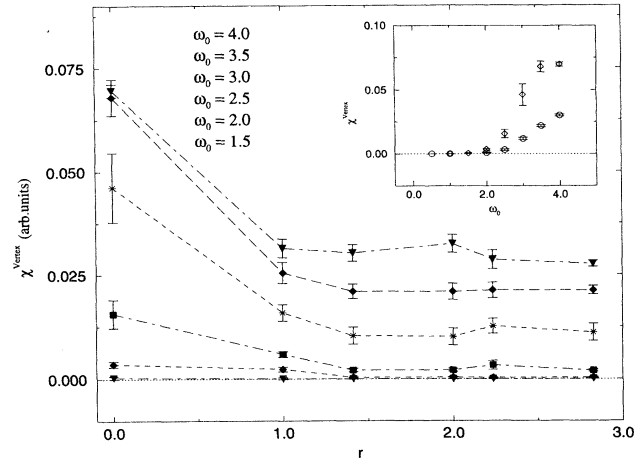


FIG. 15. The on-site  $s$ -wave pair-field correlation vertex for different values of  $\omega_0$  of a  $4 \times 4$  system with  $U=0$ ,  $g=1$ , and  $\langle n \rangle=1$  found by QMC. The inset shows the on-site value (diamonds) and the mean long-range value (circles) dependence of  $\omega_0$ .

Fig. 13. For  $g=0$  the spectral density consists of a delta peak at  $\omega=0$ . Turning on  $g$  leads to a reduction and broadening of the quasiparticle peak. In addition, structures appear at  $\pm\omega_0$  resulting from phonon (de)excitations. For sufficiently large  $g$  the spectrum becomes completely incoherent. In Fig. 14 we depict the  $U$  dependence of the electronic spectral density at half filling. Again, electronic correlations partly reverse the effect of the electron-phonon interaction. The parameters, given in the figure caption, are chosen such that the quasiparticle peak is completely swamped by the incoherent background in the  $U=0$  case. Interestingly, increasing the interelectronic correlation recovers partly the quasiparticle peak, and, also, the phonon peaks at

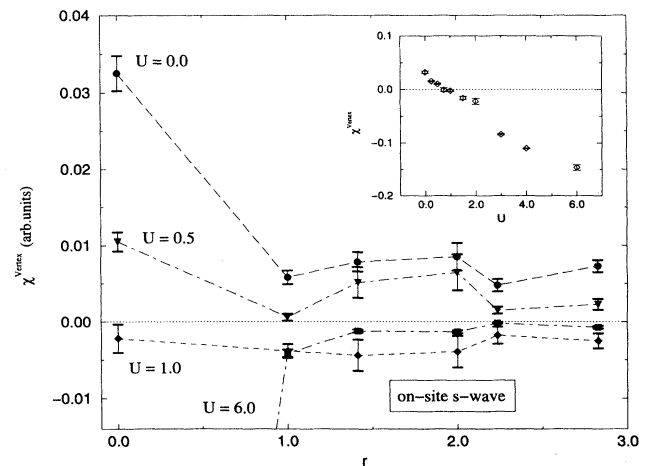


FIG. 16. The  $U$  dependence of the on-site  $s$ -wave pair-field correlation vertex of all possible lengths of a  $4 \times 4$  system with  $\omega_0=1$ ,  $g=1$ , and  $\langle n \rangle=1$  obtained by QMC. The inset shows the decreasing on-site value for different Hubbard  $U$ .

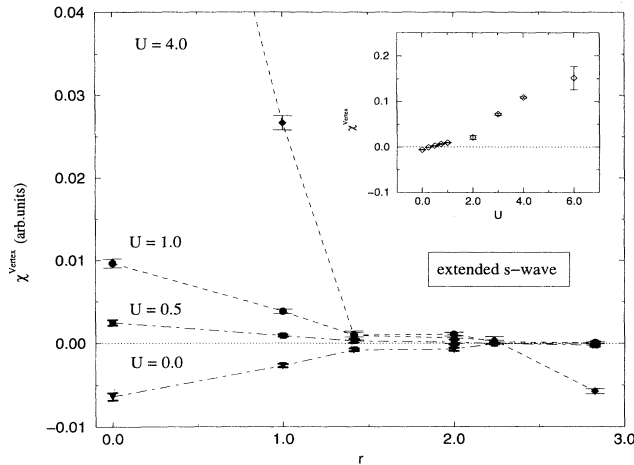


FIG. 17.  $U$  dependence of the extended  $s$ -wave pair-field correlations vertex for different lengths of a  $4 \times 4$  system with  $\omega_0=1$ ,  $g=1$ , and  $\langle n \rangle=1$  found by QMC. The inset shows the on-site value increasing with  $U$ .

$\omega = \pm\omega_0$  show up again. However, increasing  $U$  beyond  $U \approx 1$ , which corresponds to the phonon-mediated negative-effective  $U$ , leads again to a destruction of the quasiparticle features. It can be concluded from these results that the effects of the local electron-phonon coupling can to a large extent—but not entirely—be described by an effective negative Hubbard interaction. This description does not, e.g., account for the phonon (de)excitation peaks, nor does it explain the departure from a  $\delta$  peak for  $V^{\text{eff}}=0$ .

### E. Superconductivity

Supplementary to previous studies of the superconducting features of the Holstein model,<sup>5,6</sup> in which a diverging on-site  $s$ -wave pairing susceptibility has been found in the range  $g^2 < 2\omega_0$ , we performed QMC simulations to study the influence of the Coulomb repulsion. In agreement with the aforementioned diverging susceptibility, we find ODLRO in the equal-time pair-field correlation function [Eq. (17)] for on-site  $s$  waves (Fig. 15). The inset shows the increase of the on-site term and the constant value for long distances with increasing  $\omega_0$ . For  $U=0$  the vertex decreases from a large on-site value to a positive (attractive) constant for larger distances. We find that the vertex correlations for pair-field symmetries other than local  $s$  wave are negligible. It is needless to say that ODLRO in the small systems accessible by QMC studies can merely hint at the possible physical behavior of the model. Figure 16 illustrates the  $U$  dependence of the pair-field correlation vertex for the on-site  $s$ -wave channel for a different parameter set. For these parameters the system shows a strong CDW character, leading to a modulation of the  $r$  dependence of the pair-field correlation. The local repulsion  $U$  reduces charge fluctuations and leads to a strong reduction of on-site  $s$ -wave pair correlations and eventually to a repulsive interaction. At the same rate at which the attractive interaction

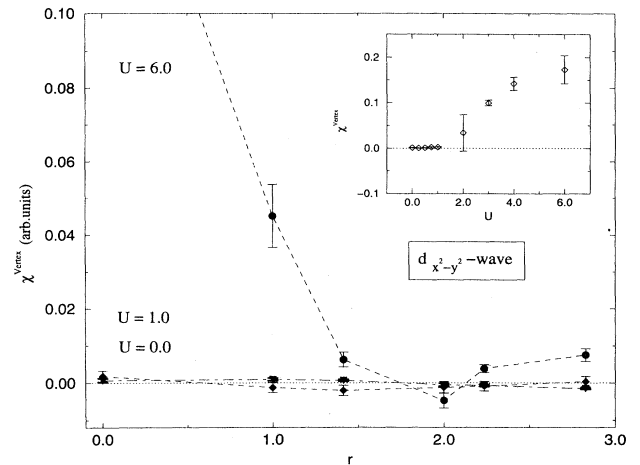


FIG. 18.  $U$  dependence of the  $d_{x^2-y^2}$ -wave pair-field correlations vertex for different lengths of a  $4 \times 4$  system with  $\omega_0=1$ ,  $g=1$ , and  $\langle n \rangle=1$  obtained by QMC. The inset shows the on-site term value increasing with  $U$ .

vanishes in the on-site  $s$ -wave channel, we observe an increasing signal in the extended  $s$ -wave (Fig. 17) and  $d$ -wave channels (Fig. 18). In spite of a strong increasing on-site value, the vertex drops to zero within one or two lattice distances in the half-filled case. In conclusion, we found no ODLRO at half filling; however, preliminary results indicate ODLRO in the  $d$ -wave channel away from half filling for  $\langle n \rangle=0.875$ . Unfortunately, the signal-to-noise ratio is poor due to the ubiquitous sign problem, and further studies are necessary for definite conclusions.

### V. SUMMARY

In summary, we performed PQMC simulations and evaluated Migdal-Eliashberg theory for the Hubbard-Holstein model. We also showed a way of calculating dynamic phonon Green's functions within the PQMC algorithm. In agreement with observations of previous studies of the bare Holstein model, we found that ME theory also yields fairly good results for the Hubbard-Holstein model if phonon renormalization and self-consistency are properly accounted for. The phonon-mediated electron-electron attraction leads to a charge-density wave and a strong renormalization of the phonon frequency. The phonon-mediated electron-electron interaction can partly be described by an effective negative- $U$  Hubbard model; but not entirely, as has been demonstrated by various dynamic properties and by the effects caused by the Hubbard interaction. It has been shown that the local Coulomb repulsion is detrimental for local  $s$ -wave pairing, while it generates attractive pairing for extended  $s$ -wave and  $d$ -wave symmetry, but no ODLRO for half filling.

### ACKNOWLEDGMENTS

We would like to thank W. Hanke, A. Muramatsu, F. Assaad, R. Hetzel, J. Gubernatis, and R. Silver for stimulating discussions.

- <sup>1</sup>T. Holstein, *Ann. Phys. (Leipzig)* **8**, 325 (1959).
- <sup>2</sup>S. Engelsberg and J. R. Schrieffer, *Phys. Rev.* **131**, 993 (1963).
- <sup>3</sup>F. Marsiglio, *Phys. Rev. B* **42**, 2416 (1990).
- <sup>4</sup>V. Meden, K. Schönhammer, and O. Gunnarsson, *Phys. Rev. B* **50**, 11 179 (1994).
- <sup>5</sup>R. T. Scalettar, N. E. Bickers, and D. J. Scalapino, *Phys. Rev. B* **40**, 197 (1989).
- <sup>6</sup>F. Marsiglio, *Physica C* **162-164**, 1453 (1989).
- <sup>7</sup>R. M. Noack, D. J. Scalapino, and R. T. Scalettar, *Phys. Rev. Lett.* **66**, 778 (1991).
- <sup>8</sup>M. Vekić, R. M. Noack, and S. R. White, *Phys. Rev. B* **46**, 271 (1992).
- <sup>9</sup>R. M. Noack, and D. J. Scalapino, *Phys. Rev. B* **47**, 305 (1993).
- <sup>10</sup>M. Vekić, R. M. Noack, and S. R. White, *Phys. Rev. B* **46**, 271 (1992).
- <sup>11</sup>M. Vekić and S. R. White, *Phys. Rev. B* **48**, 7643 (1993).
- <sup>12</sup>P. Niyaz, J. E. Gubernatis, R. T. Scalettar, and C. Y. Fong, *Phys. Rev. B* **48**, 16 011 (1993).
- <sup>13</sup>A. B. Migdal, *Zh. Eksp. Teor. Fiz.* **34**, 1438 (1958) [*Sov. Phys. JETP* **7**, 996 (1958)]; G. M. Eliashberg, *ibid.* **38**, 966 (1960) [**11**, 696 (1960)].
- <sup>14</sup>J. Ranninger and U. Thibblin, *Phys. Rev. B* **45**, 7730 (1992).
- <sup>15</sup>A.S. Alexandrov and J. Ranninger, *Phys. Rev. B* **23**, 1796 (1981); A. S. Alexandrov, J. Ranninger, and S. Robaszkiewicz, *ibid.* **33**, 4526 (1986); A. S. Alexandrov and J. Ranninger, *Physica C* **198**, 360 (1992).
- <sup>16</sup>F. Marsiglio, *Physica C* **244**, 21 (1995).
- <sup>17</sup>J. R. Schrieffer, *Theory of Superconductivity* (Benjamin, New York, 1964).
- <sup>18</sup>D. J. Scalapino, J. R. Schrieffer, and J. W. Wilkins, *Phys. Rev.* **148**, 263 (1966).
- <sup>19</sup>D. J. Scalapino, in *Superconductivity*, edited by R. D. Parks (Dekker, New York, 1969).
- <sup>20</sup>E. Berger, Diploma thesis, University Würzburg, 1994.
- <sup>21</sup>H. J. Vidberg and J. W. Serene, *J. Low Temp. Phys.* **29**, 179 (1977).
- <sup>22</sup>G. Sugiyama and S. E. Koonin, *Ann. Phys.* **168**, 1 (1986); S. Sorella, E. Tosatti, S. Baroni, R. Car, and M. Parrinello, *Towards the Theoretical Understanding of the High- $T_c$  Superconductors*, Proceedings of the Adriatico Research Conference, edited by S. Lundqvist, E. Tosatti, M. Tosi, and L. Yu (World Scientific, Singapore, 1988); S. R. White, D. J. Scalapino, R. L. Sugar, E. Y. Loh, J. E. Gubernatis, and R. T. Scalettar, *Phys. Rev. B* **41**, 9301 (1990).
- <sup>23</sup>W. v. d. Linden, *Phys. Rep.* **220**, 53 (1992), and references therein.
- <sup>24</sup>M. Frick, W. v. d. Linden, I. Morgenstern, and H. de Raedt, *Z. Phys. B* **81**, 327 (1990).
- <sup>25</sup>J. E. Hirsch, *Phys. Rev. B* **38**, 12 023 (1988).
- <sup>26</sup>P. Valášek, Diploma thesis, University Würzburg, 1993.
- <sup>27</sup>R. N. Silver, D. S. Sivia, and J. E. Gubernatis, *Phys. Rev. B* **41**, 2380 (1990).
- <sup>28</sup>J. Skilling, in *Maximum Entropy and Bayesian Methods*, edited by J. Skilling (Kluwer Academic, Dordrecht, 1989), p. 45; S. F. Gull, *ibid.*; J. Skilling, in *Maximum Entropy and Bayesian Methods*, edited by P. F. Fougère (Kluwer Academic, Dordrecht, 1990); B. Buck and V. A. Macauley, in *Maximum Entropy in Action* (Clarendon, Oxford, 1991); W. v. d. Linden, *Appl. Phys. A* **60**, 155 (1995).
- <sup>29</sup>A. O'Hagan, in *Kendall's Advanced Theory of Statistics 2B*, edited by E. Arnold (Cambridge University Press, Cambridge, 1994).
- <sup>30</sup>S. R. White, D. J. Scalapino, R. L. Sugar, and N. E. Bickers, *Phys. Rev. Lett.* **63**, 1523 (1989).